mathematics

Article

Steady Flow of Burgers' Nanofluids over a Permeable Stretching/Shrinking Surface with Heat Source/Sink

Rusya Iryanti Yahaya [1], Norihan Md Arifin [1,2,*], Ioan Pop [3], Fadzilah Md Ali [1,2] and Siti Suzilliana Putri Mohamed Isa [4]

[1] Institute for Mathematical Research, Universiti Putra Malaysia, Serdang 43400, Selangor, Malaysia; rusyairyanti@gmail.com (R.I.Y.); fadzilahma@upm.edu.my (F.M.A.)
[2] Department of Mathematics, Universiti Putra Malaysia, Serdang 43400, Selangor, Malaysia
[3] Department of Mathematics, Babeş-Bolyai University, R-400084 Cluj-Napoca, Romania; popm.ioan@yahoo.co.uk
[4] Centre of Foundation Studies for Agricultural Science, Universiti Putra Malaysia, Serdang 43400, Selangor, Malaysia; ctsuzilliana@upm.edu.my
* Correspondence: norihana@upm.edu.my

Abstract: An engineered fluid, called nanofluid, is expected to have better thermal conductivity than conventional working fluids. The superior heat transfer performance and various possible applications promote the analysis of nanofluids in different flow geometries. This paper studies the flow of non-Newtonian Burgers' nanofluids over a permeable stretching/shrinking surface with a heat source/sink. In the current study, we highlight the use of the single-phase nanofluid model in studying the boundary layer flow. The basic partial differential equations are transformed into ordinary (similarity) differential equations. Then, the resulting equations and boundary conditions are solved numerically in MATLAB using the bvp4c package. Triple solutions are presented, and stability analysis certifies that the first solution is physically realizable in practice. It is found that the increment of the heat source parameter raised the temperature profile of the nanofluids. Al_2O_3/H_2O and Cu/H_2O nanofluids produced the highest skin friction coefficient in the flow over stretching and shrinking surfaces, respectively. Meanwhile, Cu/H_2O nanofluid showed a better heat transfer performance when compared to Al_2O_3/ H_2O and TiO_2/ H_2O nanofluids. The present study is novel and could serve as a reference to other researchers for further analysis of heat transfer performance and the rheological behavior of nanofluids.

Keywords: Burgers' nanofluid; permeable surface; heat source/sink; numerical results

MSC: 76A05; 76D10; 35Q35

Citation: Yahaya, R.I.; Md Arifin, N.; Pop, I.; Md Ali, F.; Mohamed Isa, S.S.P. Steady Flow of Burgers' Nanofluids over a Permeable Stretch-Ing/Shrinking Surface with Heat Source/Sink. *Mathematics* **2022**, *10*, 1580. https://doi.org/10.3390/math10091580

Academic Editor: Antonio Lamura

Received: 7 March 2022
Accepted: 5 May 2022
Published: 7 May 2022

1. Introduction

Every fluid that obeys Newton's law of viscosity, i.e., viscosity is independent of shear stress, is termed a Newtonian fluid. Meanwhile, fluids such as toothpaste, ketchup, polymers, colloids, and tars with variable viscosity depending on the shear rate and shear stress are called non-Newtonian fluids. The non-Newtonian fluids are further classified into three sub-categories: the differential-type, integral-type, and rate-type. Fluid models such as Maxwell, Oldroyd-B, and Burgers are proposed to represent the rate-type fluids, characterized by the fluid relaxation and retardation time phenomena [1]. Among these models, only the Burgers' fluid model expresses relaxation and retardation time properties simultaneously, which is suitable for describing the rheological properties of assorted viscoelastic materials; for example, asphalt, soil, cheese, and polymeric liquids (see Hayat et al. [2]; Rashidi et al. [3]). However, the Burgers' model is less popular among researchers due to its complex constitutive equations and mathematical formulation. Some of the studies on Burgers' fluid are those by Alsaedi et al. [4], Hayat et al. [5–8], Ahmad et al. [9], Khan et al. [10], Imran et al. [11], Safdar et al. [12], Akram et al. [13], Jiang et al. [14], and Gangadhar et al. [15].

Rapid development in engineering applications and electronic devices demands a more efficient and advanced nanofluid to act as a coolant in removing excess heat from devices. Nanofluids are defined by Choi [16] as fluids containing particles with an average size of 10 nanometers (e.g., carbon nanotubes, carbides, metals, and oxides). These particles are dispersed in a conventional heat transfer fluid (e.g., water, oil, and ethylene glycol), called base fluid. The synthesis of nanofluids serves the purpose of finding superior heat transfer fluid with better performance than conventional fluids. Incorporating high thermal conductivity nanoparticles into the conventional fluids improves the heat transfer performance of the fluids (see Alghamdi [17]; Khan and Alzahrani [18]; Hayat et al. [19,20]; Iqbal et al. [21]). The processes of preparing nanofluids were elucidated by Xuan and Li [22], Das et al. [23], and Khattak et al. [24]. Due to various applications of nanofluids, for example, in manufacturing processes, microelectronics, biomedical field, food processing, nuclear cooling system, and computer processor, it is interesting to study the flow of different nanofluids over diverse physical geometries and conditions. It is worth mentioning that references to nanofluids can be found in the books by Das et al. [25], Nield and Bejan [26], Minkowycz et al. [27], and Shenoy et al. [28], and in the review papers by Manca et al. [29], Myers et al. [30], Mahian et al. [31–33], and others. Khan and Khan [34] discussed the forced convection flow of Burgers' nanofluid over a stretching sheet. Whereas Khan and Khan [35] studied the free convection flow of Burgers' nanofluid in the presence of heat generation/absorption. The effects of the heat generation parameter on the temperature profile were the opposite of the heat absorption parameter. Then, Hayat et al. [19] analyzed the flow of Burgers' nanofluid with convective boundary condition and a magnetic field. The nanofluid velocity in hydromagnetic flow was shown to be slower than in the hydrodynamic flow due to the existence of Lorentz force. Meanwhile, the relaxation and retardation time parameters reduce and enhance the velocity of the nanofluid, respectively. The same results were reported by Hayat et al. [20] for mixed convection flow. The Buongiorno nanofluid model [36] was utilized in [19,20,34,35] with thermophoresis and Brownian motion considered in these studies. Rashidi et al. [3] found that the thermophoresis and Brownian motion parameters improve the molecular movement that raises the nanofluid temperature. However, the nanofluid concentration decreases with the increment of the Brownian motion parameter. The semi-analytical solution for Burgers' nanofluid flow between parallel channels was presented by Muhammad et al. [37]. Meanwhile, the study by Khan et al. [38] and Khan et al. [1] revealed that the enhancement of thermal and concentration boundary layers was achieved through the increase of Burgers' material parameter. However, the augmentation of this parameter impedes the nanofluid velocity. Other recent studies on Burgers' nanofluid were carried out by Iqbal et al. [21], Khan et al. [39], Waqas et al. [40], Ramzan et al. [41], and Wang et al. [42].

The present study will combine the Burgers' fluid model and the single-phase Tiwari and Das [43] nanofluid model to depict the flow of nanofluids over a stretching/shrinking surface with heat generation/absorption. Flow with such geometry and conditions may have applications for heat exchangers, cooling of devices, nuclear reactors, automobiles, extrusion of plastic sheets, and many others. A previous study on Burgers' nanofluid, conducted by Khan and Khan [35], adopted the two-phase Buongiorno nanofluid model and only analyzed the stretching sheet case. Contrary to the Buongiorno model, the Tiwari and Das model considers the effects of nanoparticles volume fraction with the assumption of a no-slip condition between the nanoparticles and base fluid. The non-linear ordinary differential equations and boundary conditions will be solved numerically in MATLAB using the bvp4c package. The results, presented in tables and graphs, will be examined and discussed in detail. Through the authors' knowledge, studies on Burgers' fluid using the single-phase nanofluid model have not been carried out by other researchers. Thus, the current study is an original work to be added to the limited literature and provides new information to the researchers working in the area of nanofluids. Three different nanofluids are considered, namely Cu/H_2O, Al_2O_3/H_2O, and TiO_2/H_2O. It should be mentioned that we are able to generate triple solutions for the shrinking case ($\lambda < 0$), which doesn't exist for many shrinking problems.

2. Mathematical Model

Consider the steady flow of Burgers' fluid over a permeable stretching/shrinking surface (sheet) with heat source/sink, as shown in Figure 1. x and y are the Cartesian coordinates such that the $x-$axis runs along the surface of the sheet while the $y-$axis is in the normal direction to the sheet with the flow being at $y \geq 0$. As a thermal enhancement, three different nanoparticles, namely Cu, Al_2O_3, and TiO_2, are diluted in a base fluid (water). Assumptions are made such that the velocity of the stretching/shrinking sheet is $U_w(x)$, and the mass transfer is v_w with $v_w < 0$ for suction and $v_w > 0$ for injection. The temperature of the sheet is constant T_w, while the working fluid temperature is T_∞.

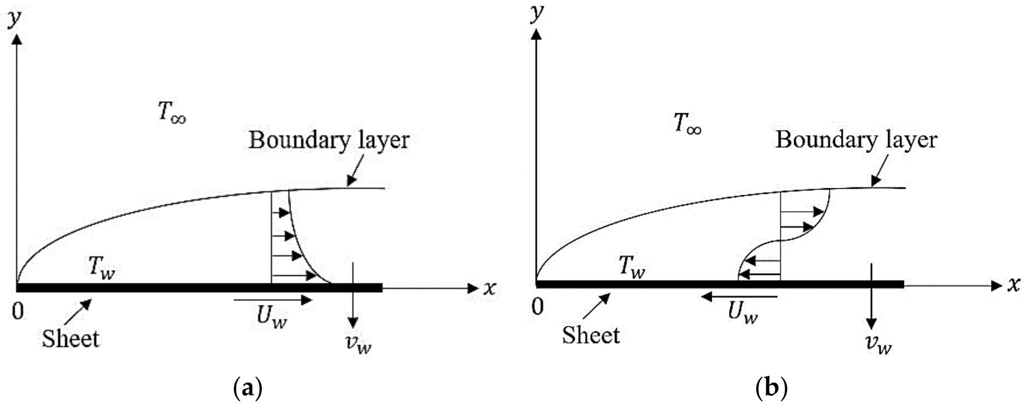

Figure 1. Physical model for: (**a**) Stretching sheet ($\lambda > 0$); (**b**) Shrinking sheet ($\lambda < 0$) [44].

The equations governing the steady boundary layer flow of an incompressible Burgers' nanofluid with a heat source/sink are written in Cartesian coordinates (x, y) as (see Khan and Khan [35]; Ejaz et al. [45]):

$$\frac{\partial u}{\partial x} + \frac{\partial v}{\partial y} = 0, \tag{1}$$

$$\left.\begin{array}{c} u\,\dfrac{\partial u}{\partial x} + v\,\dfrac{\partial u}{\partial y} + \lambda_1\left(v^2\,\dfrac{\partial^2 u}{\partial y^2} + 2\,u\,v\,\dfrac{\partial^2 u}{\partial x\,\partial y}\right) + \\ \lambda_2\left[v^3\,\dfrac{\partial^3 u}{\partial y^3} + 3\,v^2\left(\dfrac{\partial v}{\partial y}\,\dfrac{\partial^2 u}{\partial y^2} + \dfrac{\partial u}{\partial y}\,\dfrac{\partial^2 u}{\partial x\,\partial y}\right) + 3\,u\,v^2\,\dfrac{\partial^3 u}{\partial x\,\partial y^2} + \right. \\ \left. 2\,uv\,\dfrac{\partial v}{\partial y}\,\dfrac{\partial^2 u}{\partial x\,\partial y}\right] = \dfrac{\mu_n}{\rho_n}\left[\begin{array}{c} \dfrac{\partial^2 u}{\partial y^2} + \lambda_3\left(u\,\dfrac{\partial^3 u}{\partial x\,\partial y^2} + v\,\dfrac{\partial^3 u}{\partial y^3} - \right. \\ \left. \dfrac{\partial u}{\partial x}\,\dfrac{\partial^2 u}{\partial y^2} - \dfrac{\partial u}{\partial y}\,\dfrac{\partial^2 v}{\partial y^2}\right) \end{array}\right], \end{array}\right\} \tag{2}$$

$$u\,\frac{\partial T}{\partial x} + v\,\frac{\partial T}{\partial y} = \frac{k_n}{\left(\rho\,C_p\right)_n}\,\frac{\partial^2 T}{\partial y^2} + \frac{Q}{\left(\rho\,C_p\right)_n}\,(T - T_\infty), \tag{3}$$

along with the boundary conditions (see Hayat et al. [7])

$$\left.\begin{array}{c} v = v_w, \quad u = U_w(x)\,\lambda = a\,x\,\lambda, \;\; T = T_w \;\; \text{at} \;\; y = 0 \\ u \to 0, \quad \dfrac{\partial u}{\partial y} \to 0, \;\; T \to T_\infty \;\; \text{as} \;\; y \to \infty. \end{array}\right\}, \tag{4}$$

Here, u and v represent the velocity components along x −and y −axes, a is a positive constant, T is the temperature, λ_1 and λ_3 ($\leq \lambda_1$) are the relaxation and retardation times, respectively, λ_2 is the material parameter of the Burgers' fluid, Q_0 is the heat generation/absorption parameter, and λ is the constant stretching/shrinking parameter with $\lambda < 0$ for the shrinking sheet, $\lambda = 0$ for static sheet, and $\lambda > 0$ for the stretching sheet.

Next, ρ_n is the density, $(\rho C_p)_n$ is the heat capacity, μ_n is the dynamic viscosity, and k_n is the thermal conductivity of the nanofluid, given by (see Ho et al. [46]; Sheremet et al. [47]):

$$\left.\begin{array}{c} \rho_n = (1 - \phi)\,\rho_f + \phi\,\rho_s, \\ \left(\rho C_p\right)_n = (1 - \phi)\left(\rho\, C_p\right)_f + \phi\left(\rho\, C_p\right)_s, \\ \dfrac{\mu_n}{\mu_f} = \dfrac{1}{(1 - \phi)^{2.5}}, \\ \dfrac{k_n}{k_f} = \dfrac{k_s + 2\,k_f - 2\,\phi\left(k_f - k_s\right)}{k_s + 2\,k_f + 2\,\phi\left(k_f - k_s\right)}. \end{array}\right\} \tag{5}$$

Here, the suffixes f, n, and s describe the base fluid, nanofluid, and nanoparticle, respectively, ϕ is the nanoparticle volume fraction $(\phi = 0$ correspond to a regular fluid$)$, and C_p is the heat capacity at constant pressure. Table 1 describes the thermal and physical characteristics of base liquids and nanoparticles.

Table 1. Thermal and physical characteristics for nanoparticles (see Oztop and Abu Nada [48]).

Properties	ρ (kg/m³)	C_p (J/kg K)	k (W/m K)	Pr
Cu	8933	385	400	-
Al_2O_3	3970	765	40	-
TiO_2	4250	686.2	8.9538	-
H_2O	997.1	4179	0.613	6.2

Guided by the boundary conditions (4), we introduce the following similarity variables:

$$\psi = \sqrt{a\,\nu_f}\;x\,f(\eta), \qquad \theta(\eta) = \frac{T - T_\infty}{T_w - T_\infty}, \quad \eta = y\sqrt{\frac{a}{\nu_f}}, \tag{6}$$

where $\psi(x, y)$ is the Stokes stream function defined as $u = \partial\psi/\partial y$ and $v = -\partial\psi/\partial x$. Thus, we have:

$$u = a\,x\,f'(\eta), \quad v = -\sqrt{a\,\nu_f}\,f(\eta), \tag{7}$$

In addition,

$$v_w = -\sqrt{a\,\nu_f}\,S, \tag{8}$$

where prime (′) denotes differentiation with respect to η, and the mass flux parameter is S with $S < 0$ for injection and $S > 0$ for suction.

We obtain the following ordinary (similarity) differential equations after substituting (6) into Equations (2) and (3):

$$\left.\begin{array}{c}\dfrac{\mu_n/\mu_f}{\rho_n/\rho_f}f''' + f f'' - f'^2 + \beta_1(2\, f\, f' f'' - f^2 f''') + \\ \beta_2\left(f^3\, f^{iv} - 2 f f'' f'^2 - \,3\, f^2 f''^2\right) + \\ \dfrac{\mu_n/\mu_f}{\rho_n/\rho_f}\beta_3(f''^2 - f\, f^{iv}) = 0\end{array}\right\} \tag{9}$$

$$\frac{1}{Pr}\frac{k_n}{k_f}\,\theta'' + \frac{\left(\rho\, C_p\right)_n}{\left(\rho\, C_p\right)_f} f\,\theta' + K\theta = 0 \tag{10}$$

along with the boundary conditions

$$\left.\begin{array}{c} f(0) = S, \qquad f'(0) = \lambda, \quad \theta(0) = 1 \\ f'(\eta) \to 0, \quad f''(\eta) \to 0, \quad \theta(\eta) \to 0 \quad \text{as} \quad \eta \to \infty \end{array}\right\} \tag{11}$$

Here, Pr is the Prandtl number, β_1, β_2 and β_3 are the non-Newtonian parameters, and $K > 0$ is the heat source and $K < 0$ is the heat sink, which are defined as:

$$Pr = \frac{(\mu\, C_p)_f}{k_f}, \;\; \beta_1 = a\,\lambda_1, \;\; \beta_2 = \, a^2\,\lambda_2, \;\; \beta_3 = a\,\lambda_3, \;\; K = \frac{Q_0}{a\,(\rho C_p)_f} \tag{12}$$

The quantities of physical interest are the skin friction coefficient (C_f) and the local Nusselt number (Nu_x):

$$C_f \,=\, \frac{\mu_n}{\rho_f[U_w(x)]^2}\left(\frac{\partial\, u}{\partial\, y}\right)_{y=0}, \qquad Nu_x = \frac{x\, k_n}{k_f\,(T_w \,-\, T_\infty)}\left(-\frac{\partial\, T}{\partial\, y}\right)_{y=0}. \tag{13}$$

Using (7) and (13), we acquire:

$$Re_x^{1/2} C_f = \frac{\mu_n}{\mu_f} f''(0), \qquad Re_x^{-1/2} Nu_x \,=\, -\frac{k_n}{k_f}\,\theta'(0) \tag{14}$$

It is worth mentioning that for $\phi = 0$ (classical viscous fluid) and $\beta_1 = \beta_2 = \beta_3 = 0$, Equation (9) becomes identical with Equation (7) from the paper by Fang et al. [49], namely,

$$f''' + f f'' - f'^2 = 0 \tag{15}$$

along with the boundary conditions,

$$f(0) = S, \qquad f'(0) = \,\lambda, \quad f'(\eta) \to 0 \quad \text{as} \quad \eta \to \infty. \tag{16}$$

The exact solution of the boundary value problem (15,16) is given by Vajravelu and Rollings [50] or Cortell [51], as,

$$f(\eta) = S + \,\alpha\left(1 - \,e^{-\beta\,\eta}\right), \;\; \beta = S + \,\alpha > 0 \tag{17}$$

where $\alpha\,\beta = \lambda$, from the boundary condition $f'(0) = \lambda$. The value β (>0) is given by the quadratic equation,

$$\beta^2 - S\,\beta - \,\lambda = 0 \tag{18}$$

and then,

$$\beta = \frac{S \;\pm\; \sqrt{S^2 \,+\, 4\,\lambda}}{2} \tag{19}$$

Thus, we have,

$$f''(0) = -\,\frac{\lambda}{2}\left(S \pm \sqrt{S^2 + 4\,\lambda}\right) \tag{20}$$

so that it gives, as it is expected, $\lambda_c = \,-S^2/4 \,<\, 0$, where λ_c is the critical value of λ (< 0) for which the boundary value problem (15) and (16) has a physical realizable problem.

Further, we notice that when $\lambda = 1$ (stretching sheet) and $S = 0$ (impermeable surface), we acquire from (20) that $f''(0) = -1$, which is in agreement with the value first reported by Crane [52].

3. Stability Analysis

The multiple solutions to the boundary value problem (9)–(11) are classified as stable or unstable by performing a stability analysis. Weidman et al. [53] and Roşca and Pop [54] have shown in their respective studies that the lower branch solutions are unstable (not realizable physically), while the upper branch solutions are stable (physically realizable). The stability analysis of multiple solutions had also been conducted in the papers by Wahid et al. [55], Lund et al. [56], and Yahaya et al. [57]. As in Weidman et al. [53], we introduce a new dimensionless time variable $\tau = at$ with t as time. The involvement of τ corresponds to an initial value problem and is suitable with the uncertainty of which solution is physically realizable. Numerical computations of boundary layer problem (9)–(11) may produce zero, unique, or multiple solutions. Therefore, the governing Equations (9) and (10) are replaced by unsteady boundary layer equations and new similarity variables containing a dimensionless time variable τ. Then, we obtain:

$$\begin{gathered}\frac{\mu_n/\mu_f}{\rho_n/\rho_f}\frac{\partial^3 f}{\partial\eta^3}+f\frac{\partial^2 f}{\partial\eta^2}-\left(\frac{\partial f}{\partial\eta}\right)^2+\beta_1\left[2f\frac{\partial f}{\partial\eta}\frac{\partial^2 f}{\partial\eta^2}-f^2\frac{\partial^3 f}{\partial\eta^3}\right]+\beta_2\left[f^3\frac{\partial^4 f}{\partial\eta^4}-\right.\\ \left.3f^2\left(\frac{\partial^2 f}{\partial\eta^2}\right)^2-2f\left(\frac{\partial f}{\partial\eta}\right)^2\frac{\partial^2 f}{\partial\eta^2}\right]+\frac{\mu_n/\mu_f}{\rho_n/\rho_f}\beta_3\left[\left(\frac{\partial^2 f}{\partial\eta^2}\right)^2-f\frac{\partial^4 f}{\partial\eta^4}\right]-\frac{\partial^2 f}{\partial\eta\,\partial\tau}=0,\end{gathered}\tag{21}$$

$$\frac{1}{Pr}\frac{k_n}{k_f}\frac{\partial^2\theta}{\partial\eta^2}+\frac{(\rho\,C_p)_n}{(\rho\,C_p)_f}f\frac{\partial\theta}{\partial\eta}+K\,\theta-\frac{(\rho\,C_p)_n}{(\rho\,C_p)_f}\frac{\partial\theta}{\partial\tau}=0,\tag{22}$$

$$\left.\begin{array}{c}f(0,\tau)=0,\quad \dfrac{\partial f}{\partial\tau}(0,\tau)=0,\quad \theta(0,\tau)=0\\ \dfrac{\partial f}{\partial\eta}(\eta,\tau)\to 0,\quad \dfrac{\partial^2 f}{\partial\eta^2}(\eta,\tau)\to 0,\quad \theta(\eta,\tau)\to 0\ \text{ as }\ \eta\to\infty\end{array}\right\}.\tag{23}$$

To test the stability of the steady flow solutions $f(\eta) = f_0(\eta)$ and $\theta(\eta) = \theta_0(\eta)$ satisfying the boundary-value problem (9)–(11), we can write (see Weidman et al. [53] and Roşca and Pop [54]),

$$\left.\begin{array}{l}f(\eta,\tau)=f_0(\eta)+e^{-\gamma\tau}\,F(\eta,\tau)\\ \theta(\eta,\tau)=\theta_0(\eta)+e^{-\gamma\tau}\,G(\eta,\tau)\end{array}\right\}\tag{24}$$

where γ is an unknown eigenvalue parameter related to the growth and decay distributions of disturbance, and $f(\eta) = f_0(\eta)$ and $\theta(\eta) = \theta_0(\eta)$ with $F(\eta,\tau) \ll f_0(\eta)$ and $G(\eta,\tau) \ll \theta_0(\eta)$.

The stability of solutions is determined by detecting the presence of initial growth or decay of disturbance in the solutions. Thus, the value of τ is set to zero so that $F(\eta) = F_0(\eta)$ and $G(\eta) = G_0(\eta)$, and the following linear eigenvalue problem is obtained:

$$\begin{gathered}\frac{\mu_n/\mu_f}{\rho_n/\rho_f}F_0'''+f_0\,F_0''+F_0\,f_0''-2\,F_0'\,f_0'+\beta_1\,[2\,f_0\,f_0'\,F_0''+2\,f_0\,F_0'\,f_0''+2\,F_0\,f_0'\,f_0''\\ -f_0^2\,F_0'''-2\,f_0\,F_0\,f_0''']+\beta_2\left[f_0^3\,F_0''''+3\,f_0^2\,F_0\,f_0''''-6\,f_0^2\,f_0''\,F_0''-6\,f_0\,F_0\,f_0''^2\right.\\ \left.-2\,f_0\,f_0'^2\,F_0''-4\,f_0\,f_0'\,f_0''\,F_0'-2\,F_0\,f_0'^2\,f_0''\right]+\frac{\mu_n/\mu_f}{\rho_n/\rho_f}\beta_3\,[2\,f_0''\,F_0''-f_0\,F_0''''-F_0\,f_0'''']+\gamma F_0'=0,\end{gathered}\tag{25}$$

$$\frac{1}{Pr}\frac{k_n}{k_f}G_0''+\frac{(\rho\,C_p)_n}{(\rho\,C_p)_f}[f_0\,G_0'+F_0\,\theta_0']+K\,G_0+\frac{(\rho\,C_p)_n}{(\rho\,C_p)_f}\gamma\,G_0=0,\tag{26}$$

with the linearized boundary conditions:

$$\left.\begin{array}{c} F_0(0) = 0, \quad F_0'(0) = 0, \quad G_0(0) = 0 \\ F_0'(\infty) \to 0, \quad F_0''(\infty) \to 0, \quad G_0(\infty) \to 0 \end{array}\right\}. \tag{27}$$

The free-stream boundary condition $F_0'(\infty) \to 0$ is relaxed so that a possible range of eigenvalues, with the smallest eigenvalue of γ_1, can be generated in the numerical computation (see Harris et al. [58] and Zainal et al. [59]). Hence, Equations (25) and (26) are solved numerically with a new set of boundary conditions:

$$\left.\begin{array}{c} F_0(0) = 0, \quad F_0'(0) = 0, \quad F_0''(0) = 1, \quad G_0(0) = 0 \\ F_0''(\infty) \to 0, \quad G_0(\infty) \to 0 \end{array}\right\} \tag{28}$$

4. Results and Discussion

All numerical computations are conducted using the bvp4c package containing finite difference code that utilizes the three-stage Lobatto IIIa formula. Equations (9), (10), (25), and (26) with the boundary conditions (11) and (28) are converted into the bvp4c algorithm. The examples are shown by Khashi'ie et al. [60] and Yahaya et al. [61]. Most of the time, the controlling parameters are kept constant with values of $\phi = 0.2, \lambda = -1, S = 3, K = 0.2, \beta_1 = 0.4, \beta_2 = 0.3$ and $\beta_3 = 0.1$. The finite value for the free-stream boundary conditions (11) (i.e., $\eta \to \infty$) is adjusted such that $\eta_{\max} = 7$ to match the specified values of the controlling parameters. All profiles successfully achieve the free-stream condition (11) within the range of the stated $\eta_{\max}$. Following Pantokratoras [62], the velocity and temperature profiles should reach the free-stream boundary condition with asymptotic behavior to satisfy the boundary layer flow. Thus, ensuring the correctness of the numerical computations and results. To be confident, we compared the present numerical results with a published study, as shown in Table 2. Again, the results show a good agreement.

Table 2. Comparison on the values of $-f''(0)$ when $\phi = 0, \lambda = 1, S = 0, K = 0$ and $\beta_2 = \beta_3 = 0$.

$\boldsymbol{\beta_1}$	$-\boldsymbol{f''(0)}$	
	Present Study	**Hayat et al. [8]**
0	1.000000	1.000000
0.2	1.051890	1.051889
0.4	1.101903	1.101903
0.6	1.150137	1.150137

At the value of $\lambda = -1$, which denotes a shrinking sheet case, triple solutions are found and assigned as the first, second, and third solutions following the arrival of each to the free-stream boundary condition (11). The numerical results of the linear eigenvalue problem (25), (26), and (28) for the smallest eigenvalue, γ_1, are tabulated in Table 3. Based on these results, there is an initial decay of disturbance (i.e., $\gamma_1 > 0$) in the first solution, whereas an initial growth (i.e., $\gamma_1 < 0$) is detected in the second and third solutions (see Yahaya et al. [57]). Therefore, the first solution is stable, while the second and third solutions are unstable. The first solution will be meaningful and realizable in real-life applications. Hence, the discussion in this section will focus on the first solution. Nevertheless, the other solutions are still recorded due to their mathematical importance.

Table 3. Values of γ_1 for various nanofluid when $\phi = 0.2, \lambda = -1, S = 3, K = 0.2, \beta_1 = 0.4, \beta_2 = 0.3$ and $\beta_3 = 0.1$.

Nanofluid	γ_1		
	First Solution	Second Solution	Third Solution
Cu/H_2O	0.3009	−0.2486	−0.3246
Al_2O_3/H_2O	0.5468	−0.1424	−0.4223
TiO_2/H_2O	0.5254	−0.1544	−0.3289

In this study, different nanoparticles are dispersed in a base fluid to form three different nanofluids, named Cu/H_2O (copper-water), Al_2O_3/H_2O (aluminum oxide-water), and TiO_2/H_2O (titanium dioxide-water) nanofluids. The skin friction coefficient ($Re_x^{1/2}C_f$) and Nusselt number ($Re_x^{-1/2}Nu_x$) of these nanofluids are compared in Table 4. At the selected values of controlling parameters, the skin friction coefficient varies slightly between the nanofluids. However, Al_2O_3/H_2O and Cu/H_2O nanofluids are perceived to have the largest value of $Re_x^{1/2}C_f$ in the stretching and shrinking cases, respectively. In addition to that, the skin friction coefficient is higher in the shrinking sheet case than in the stretching sheet case, and $Re_x^{1/2}C_f > 0$ indicates the fluid exerts a drag force on the sheet. Meanwhile, the Nusselt number, related to heat transfer rate, is enhanced significantly when Cu nanoparticle is used for the nanofluid. It is observed that Cu/H_2O nanofluid has the highest value of $Re_x^{-1/2}Nu_x$ compared to other nanofluids, and the rate of heat transfer in the stretching sheet case is slightly higher than in the shrinking sheet case. The comparison of the Nusselt number produced by these nanoparticles when dispersed in a Newtonian base fluid (water) was performed by Rahman and Ariz [63] and Dawar et al. [64]. The combination Cu/H_2O nanofluid also displays the highest Nusselt number in these studies. As tabulated in Table 1, Cu nanoparticles has the highest thermal conductivity (k), which explains the largest increment of $Re_x^{-1/2}Nu_x \left(= -\frac{k_n}{k_f}\,\theta'(0)\right)$ occurred with the mixture of water and Cu nanoparticles. However, the combination of water and Cu nanoparticles augments the skin friction coefficient in the shrinking sheet case. Whereas Cu/H_2O nanofluid produces the lowest skin friction coefficient in the stretching sheet case.

Table 4. Values of $Re_x^{1/2}C_f$ and $Re_x^{-1/2}Nu_x$ for various nanofluid when $\phi = 0.2, S = 3, K = 0.2, \beta_1 = 0.4, \beta_2 = 0.3$ and $\beta_3 = 0.1$.

λ	Nanofluid	$Re_x^{1/2}C_f$			$Re_x^{-1/2}Nu_x$		
		First Solution	Second Solution	Third Solution	First Solution	Second Solution	Third Solution
1	Cu/H_2O	0.174834	-	-	18.530621	-	-
	Al_2O_3/H_2O	0.184990	-	-	18.148114	-	-
	TiO_2/H_2O	0.184073	-	-	17.977145	-	-
−1	Cu/H_2O	0.834006	0.813087	0.537593	16.965115	16.963347	16.939337
	Al_2O_3/H_2O	0.823040	0.800393	0.640871	16.639103	16.637469	16.625451
	TiO_2/H_2O	0.820846	0.798131	0.628143	16.647590	16.646339	16.636665

The velocity and temperature profiles of various nanofluids are presented in Figures 2 and 3. From Figure 2, it is found that Al_2O_3/H_2O and Cu/H_2O have the highest and lowest velocity profiles, respectively. Meanwhile, the thermal boundary layer of Cu/H_2O nanofluid is thicker than the other nanofluids, as depicted in Figure 3. The high thermal conductivity of Cu nanoparticles is enough to increase the Nusselt number of the nanofluid even with a small temperature gradient ($-\theta'(0)$).

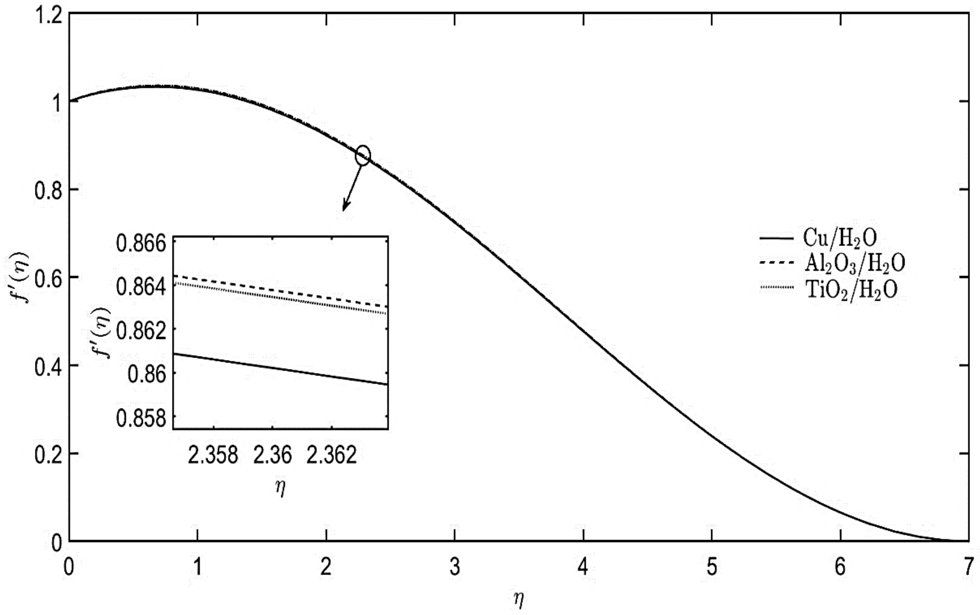

(**a**)

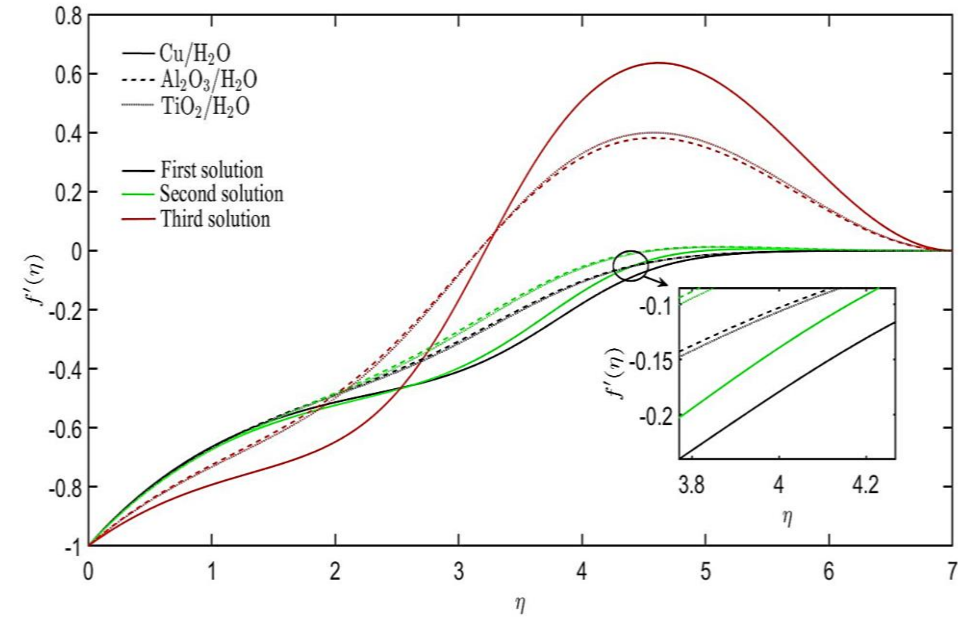

(**b**)

Figure 2. Velocity profiles of different nanofluids for: (**a**) Stretching case; (**b**) Shrinking case.

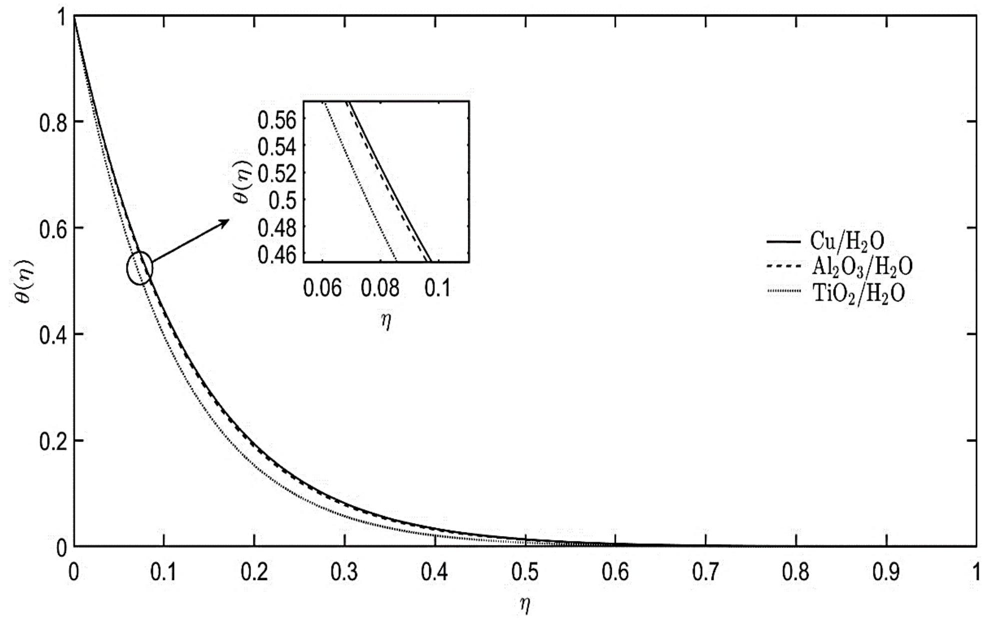

(**a**)

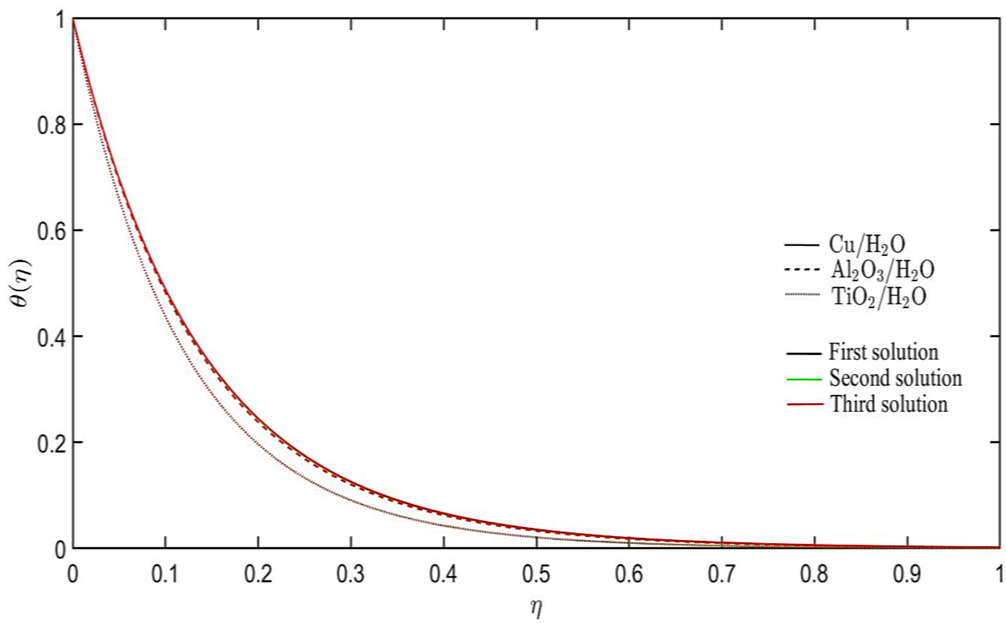

(**b**)

Figure 3. Temperature profiles of different nanofluids for: (**a**) Stretching case; (**b**) Shrinking case.

Next, the effects of nanoparticle volume fraction (ϕ) are presented in Figures 4 and 5. In both cases of stretching and shrinking sheets, the rise of ϕ improves the velocity and temperature profiles of the nanofluids. Physically, the addition of ϕ raises the collision of nanoparticles and base fluid which accelerates the nanofluid velocity [64]. As the value of ϕ increases, the momentum and thermal boundary layers enlarge. Then, the temperature gradient ($-\theta'(0)$) decreases. However, the increment of nanoparticle volume fraction boosts the thermal conductivity of the nanofluids that augments the Nusselt number $\left(Re_x^{-1/2}Nu_x = -\frac{k_n}{k_f}\,\theta'(0)\right)$ associated with the heat transfer rate.

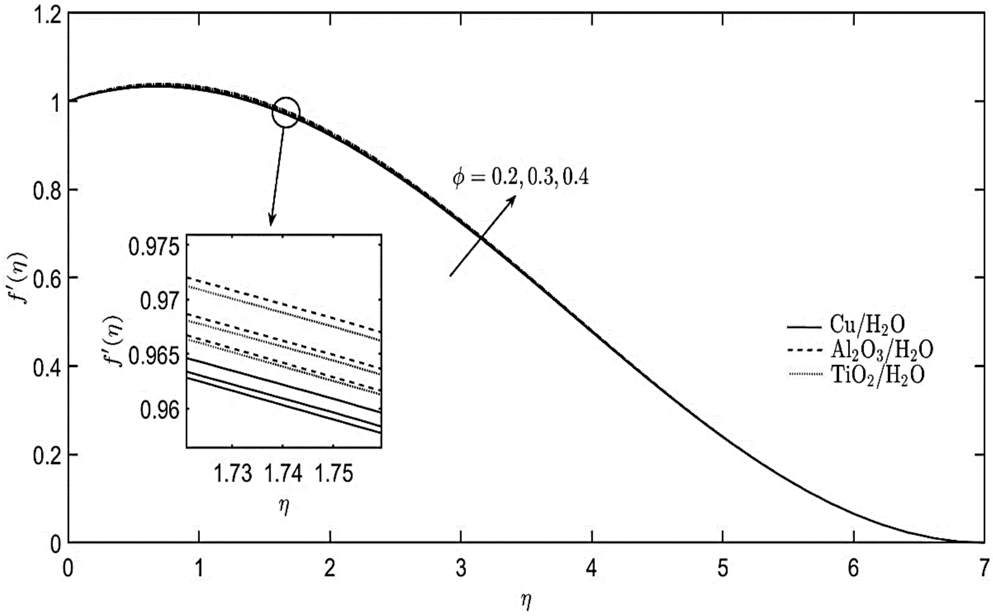

(**a**)

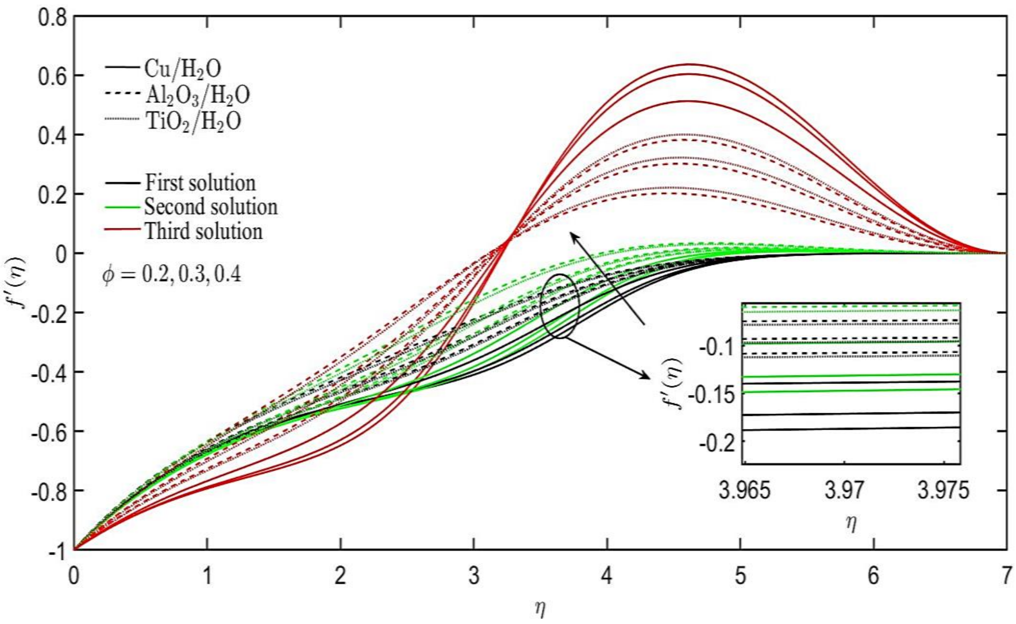

(**b**)

Figure 4. Effect of nanoparticle volume fraction on velocity profiles for: (**a**) Stretching case; (**b**) Shrinking case.

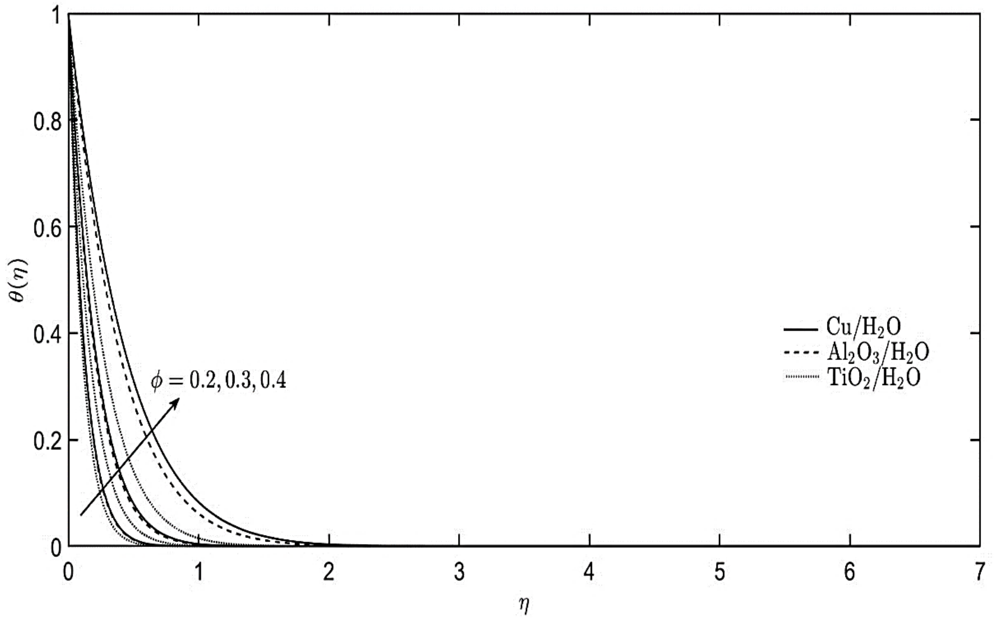

(**a**)

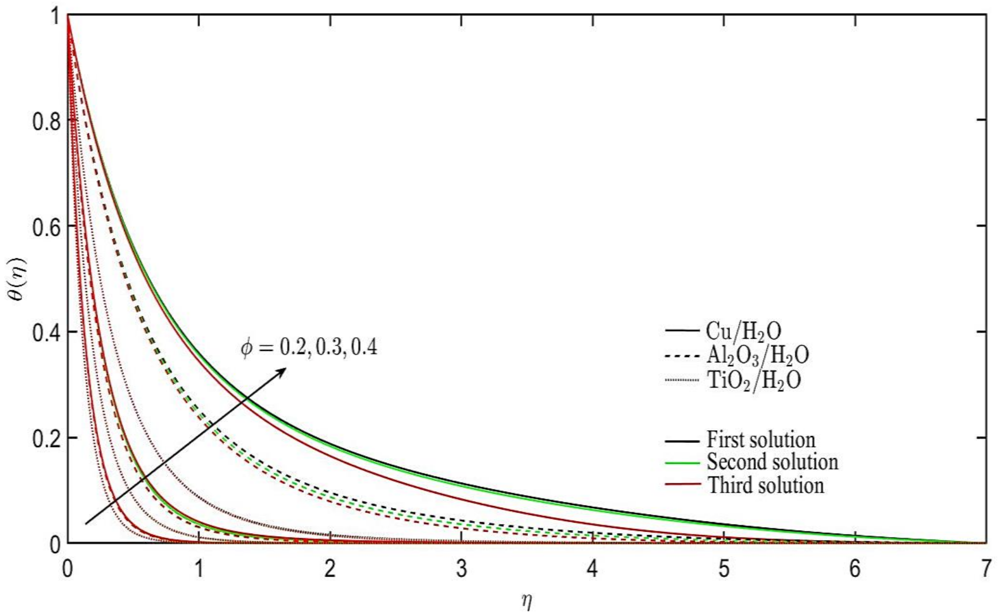

(**b**)

Figure 5. Effect of nanoparticle volume fraction on temperature profiles for: (**a**) Stretching case; (**b**) Shrinking case.

The temperature profiles with various values of heat source/sink parameter (K) are shown in Figure 6. It is observed that the increment of heat source parameter ($K > 0$) raises the temperature profiles of the nanofluids. The presence of a heat source yields extra heat to the nanofluids and raises the temperature. The thermal boundary layer thickness is also increased by $K(> 0)$. However, the enhancement in the heat sink parameter ($K < 0$) reduces the temperature profiles and thermal boundary layer thickness. These agree with the results obtained by Khan and Khan [35].

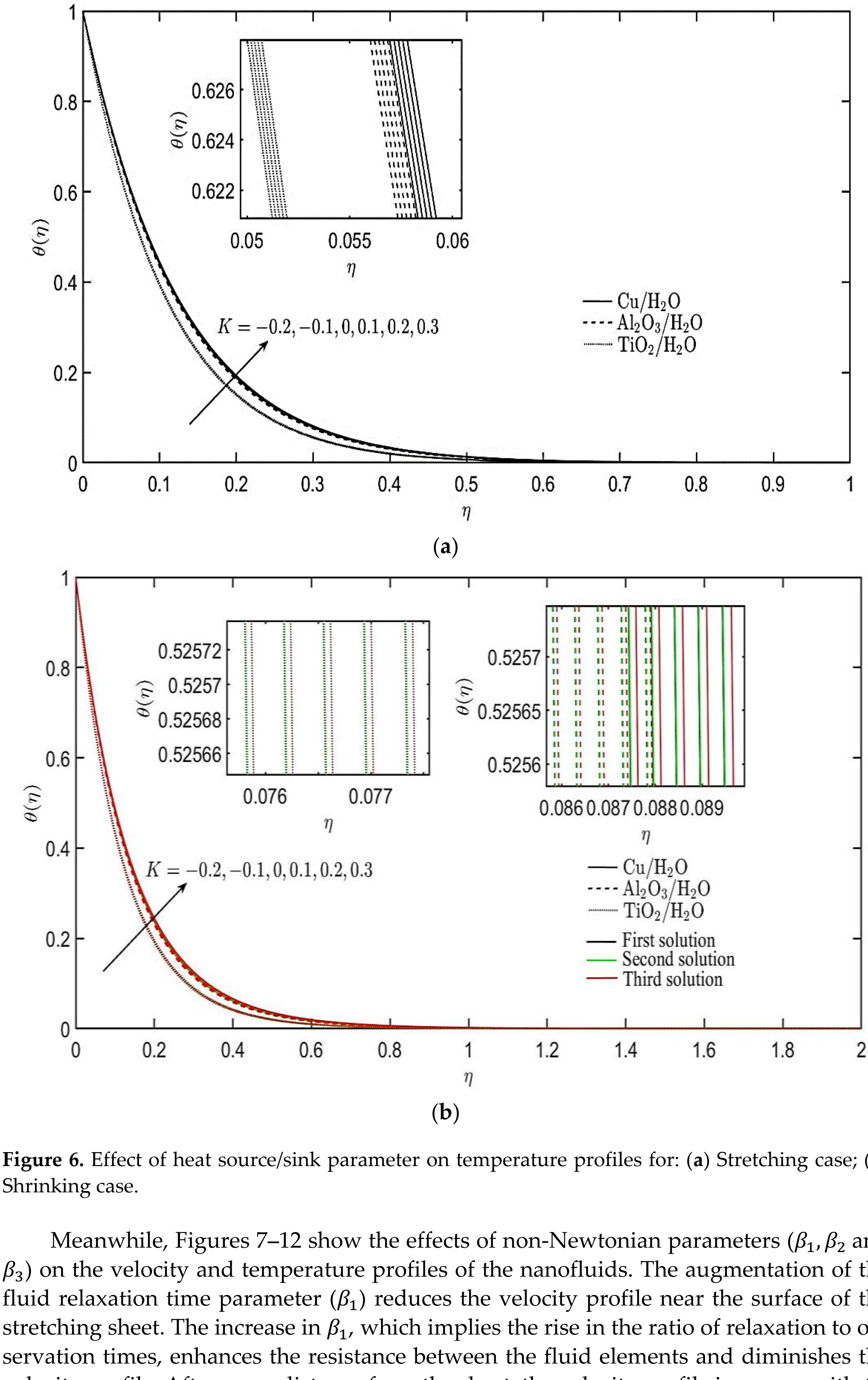

Figure 6. Effect of heat source/sink parameter on temperature profiles for: (**a**) Stretching case; (**b**) Shrinking case.

Meanwhile, Figures 7–12 show the effects of non-Newtonian parameters (β_1, β_2 and β_3) on the velocity and temperature profiles of the nanofluids. The augmentation of the fluid relaxation time parameter (β_1) reduces the velocity profile near the surface of the stretching sheet. The increase in β_1, which implies the rise in the ratio of relaxation to observation times, enhances the resistance between the fluid elements and diminishes the velocity profile. After some distance from the sheet, the velocity profile increases with β_1. Since resistance generates heat, the temperature profile rises with the increment of β_1. However, the opposite behaviors are observed for the shrinking sheet case illustrated in Figures 7b and 8b. The Burgers' fluid parameter (β_2) exhibits the same effects as β_1 on the velocity and temperature profiles of the nanofluids. According to Hayat et al. [6], β_1 and β_2 demonstrate both viscous and elastic effects, which give rise to tensile stress that reduces the velocity and momentum boundary layer thickness, as obtained in Figure 9a.

Furthermore, β_2 is also dependent on relaxation time which raises the temperature profile displayed in Figure 10a. In contrast, the profiles for the shrinking sheet case, in Figures 9b and 10b, revealed different behaviors from the stretching sheet case. In Figures 11a and 12a, the fluid retardation time parameter (β_3) boosts the velocity profile of the nanofluids but lowers the temperature profile. Retardation time implies the specific time needed to build shear stress in the fluid (see Iqbal et al. [21]). Hence, the increase in β_3 yields more shear stress and improves the fluid velocity. The thinning of the thermal boundary layer raises the temperature gradient for a better heat transfer rate. However, the opposite occurred for the shrinking sheet case in Figures 11b and 12b.

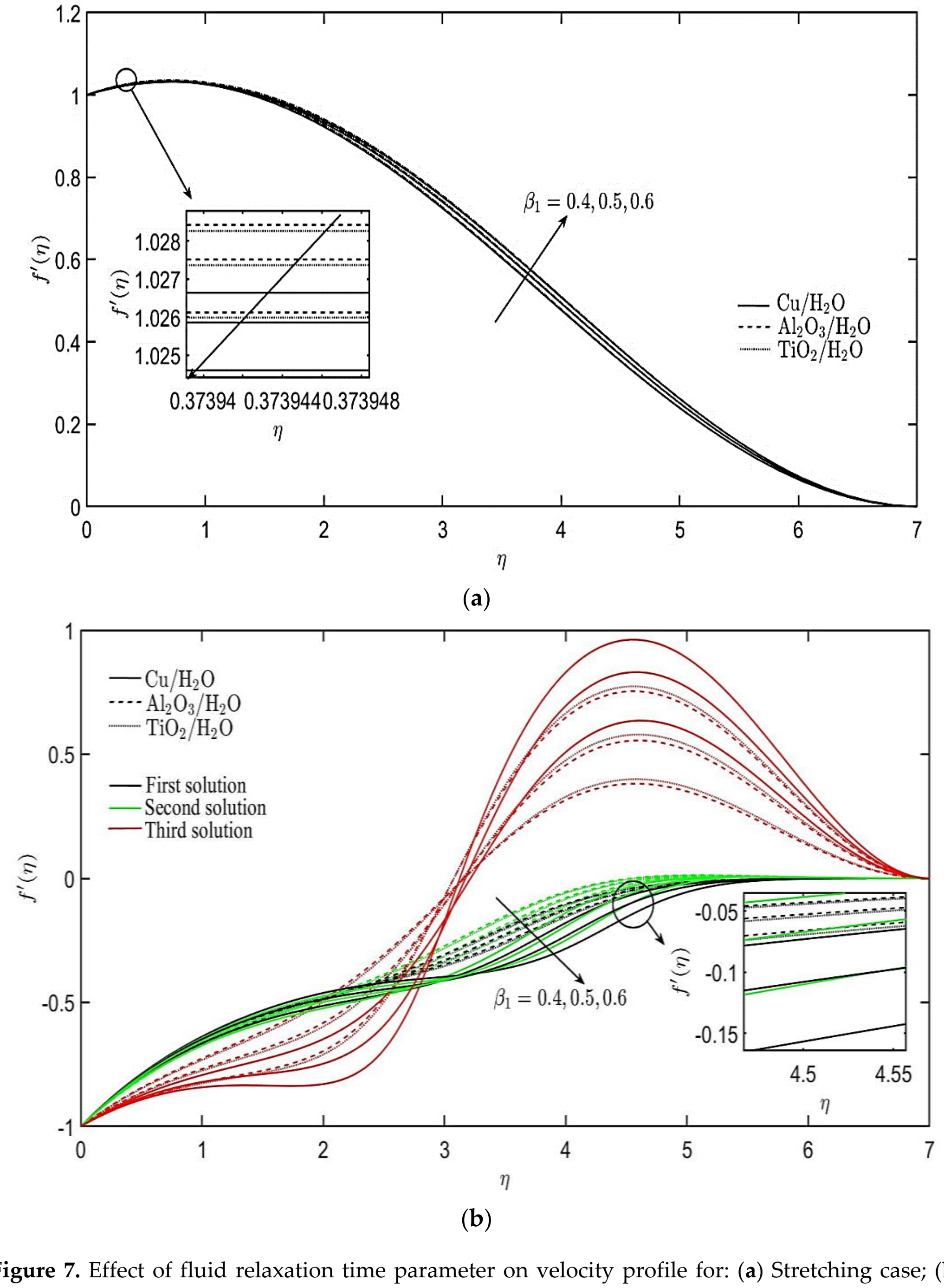

Figure 7. Effect of fluid relaxation time parameter on velocity profile for: (**a**) Stretching case; (**b**) Shrinking case.

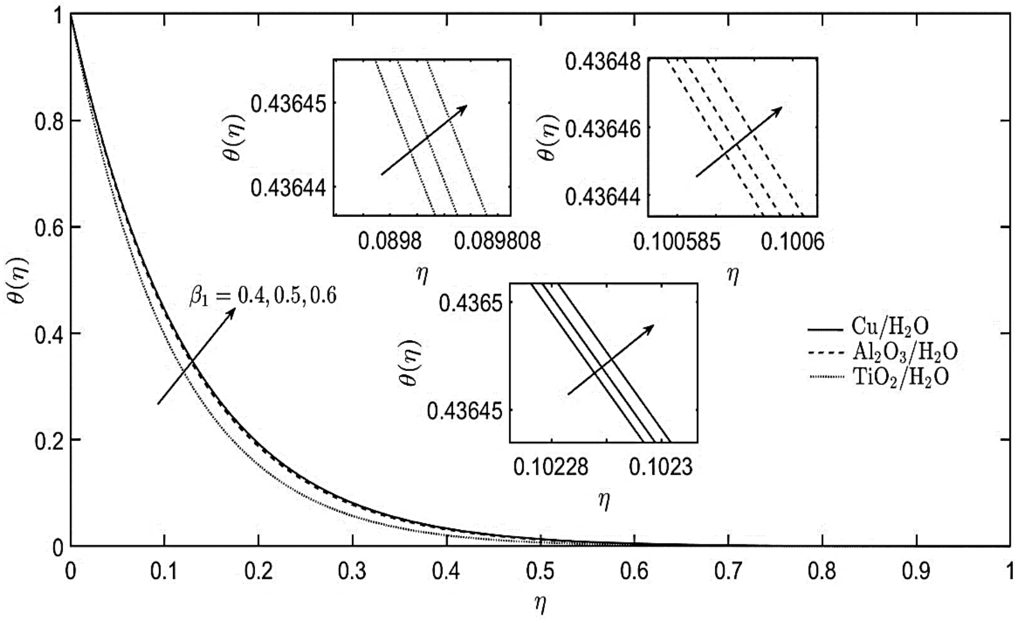

(**a**)

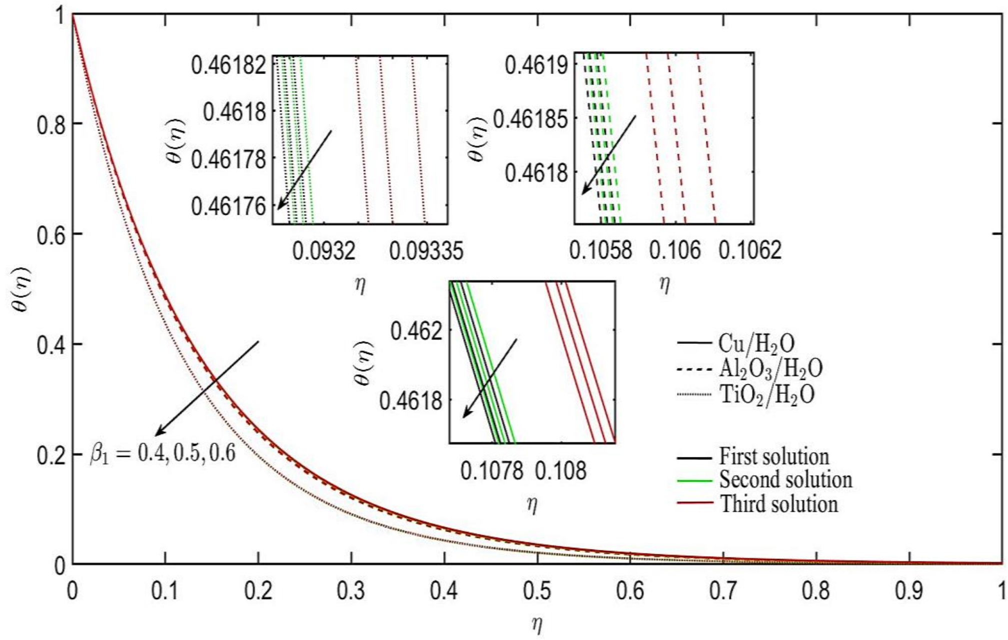

(**b**)

Figure 8. Effect of fluid relaxation time parameter on temperature profiles for: (**a**) Stretching case; (**b**) Shrinking case.

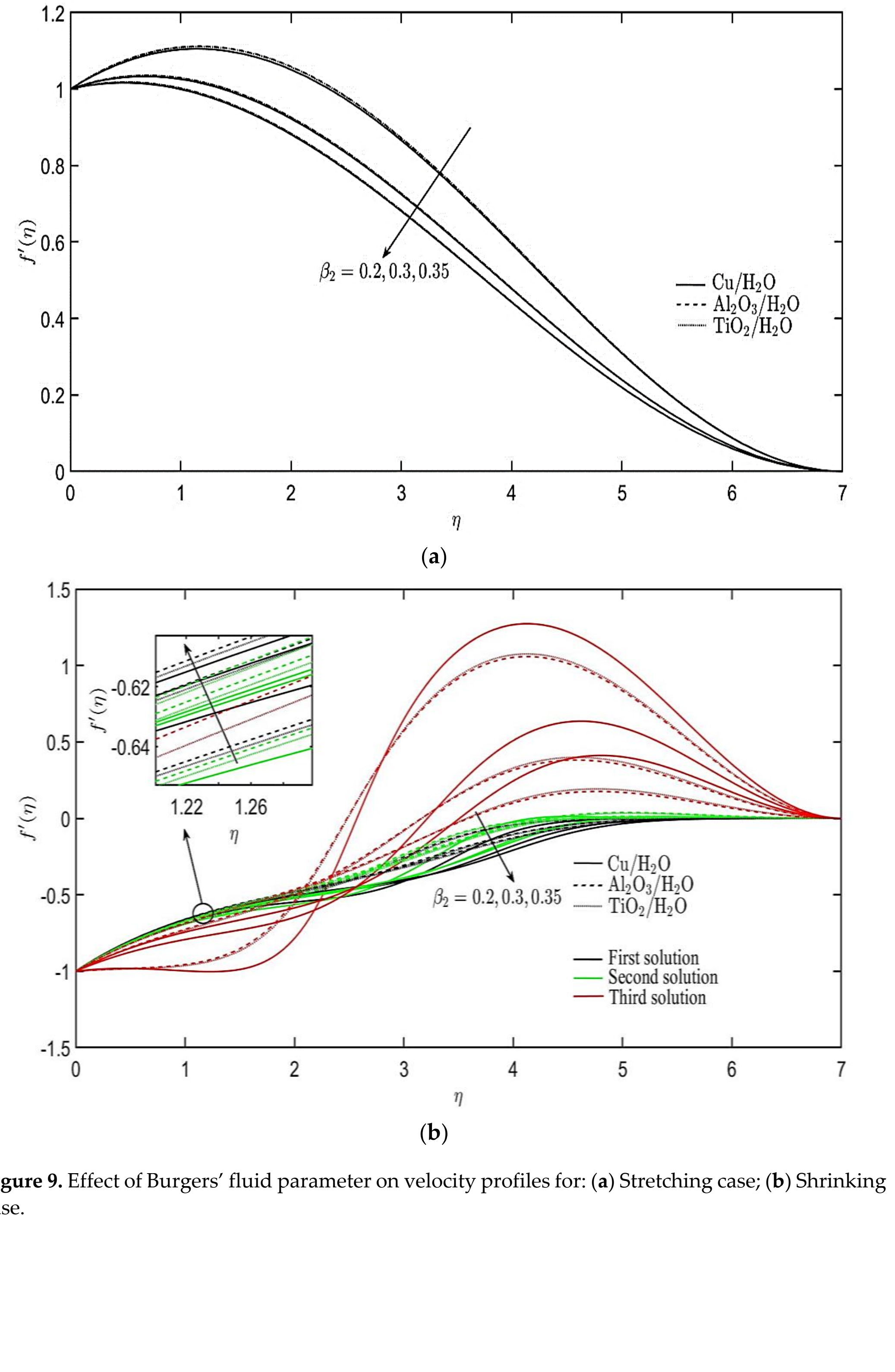

Figure 9. Effect of Burgers' fluid parameter on velocity profiles for: (**a**) Stretching case; (**b**) Shrinking case.

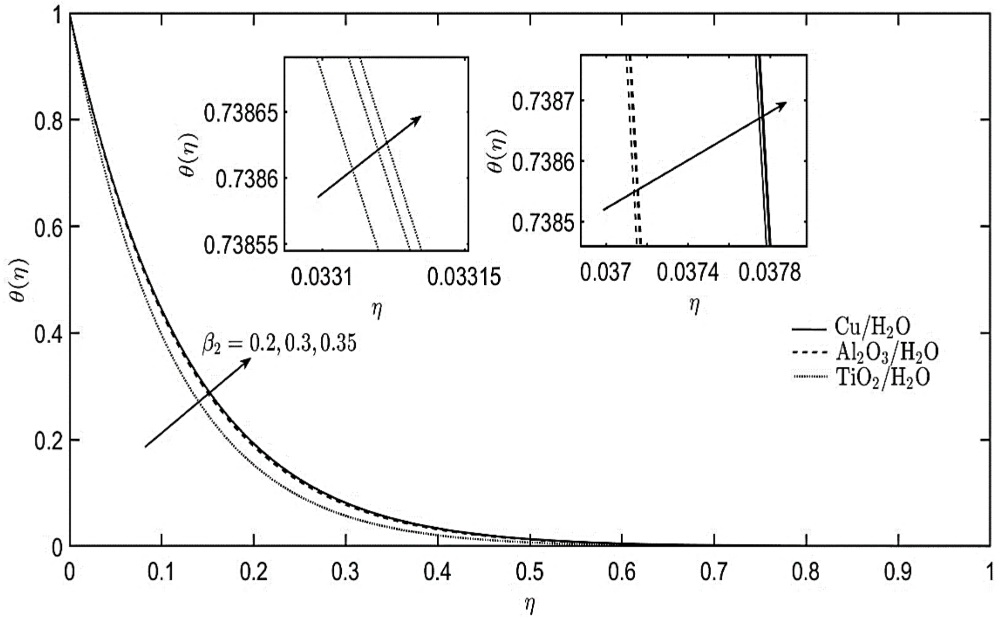

(**a**)

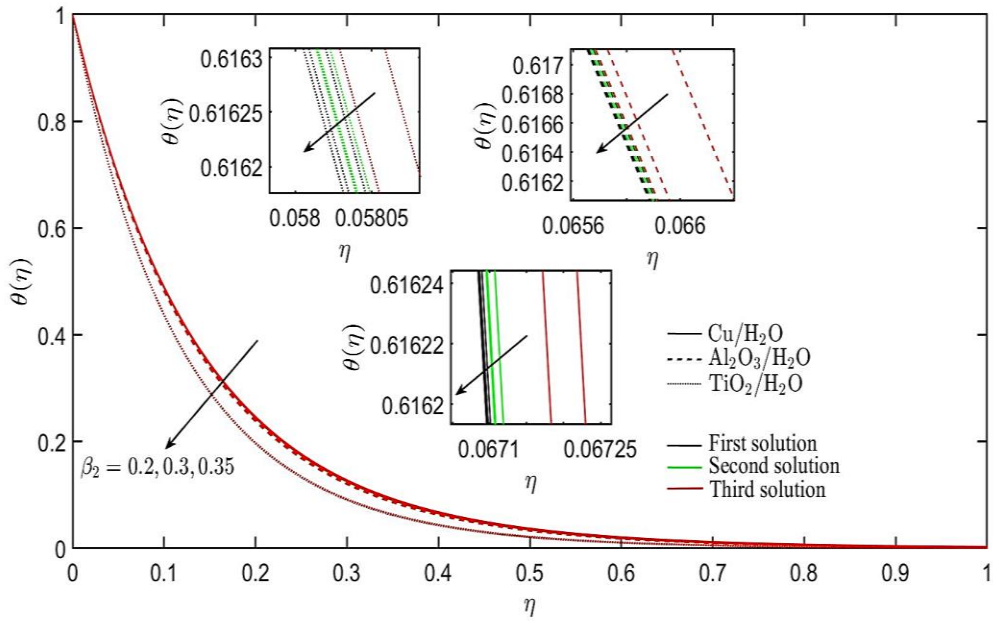

(**b**)

Figure 10. Effect of Burgers' fluid parameter on temperature profiles for: (**a**) Stretching case; (**b**) Shrinking case.

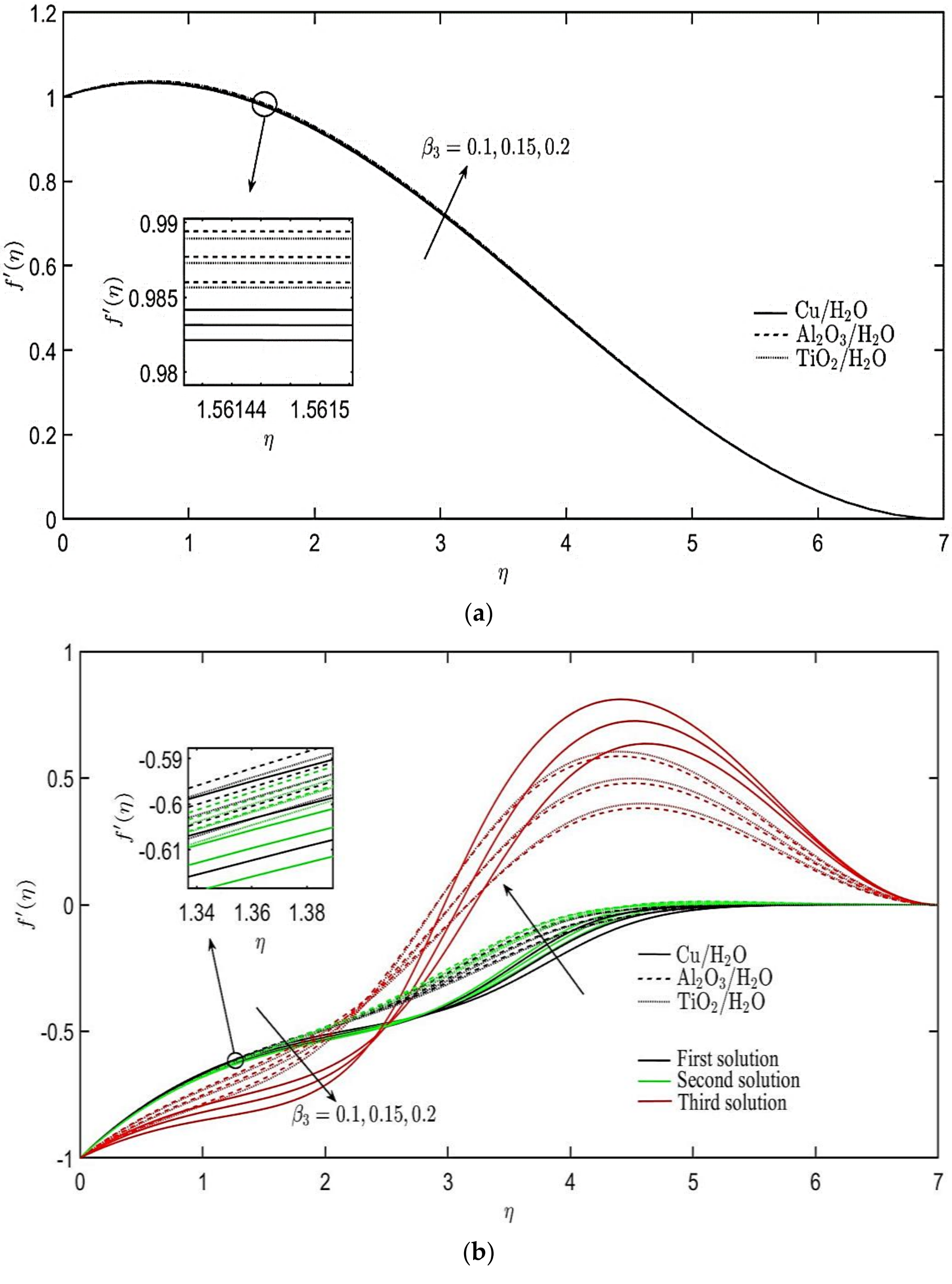

Figure 11. Effect of fluid retardation time parameter on velocity profiles for: (**a**) Stretching case; (**b**) Shrinking case.

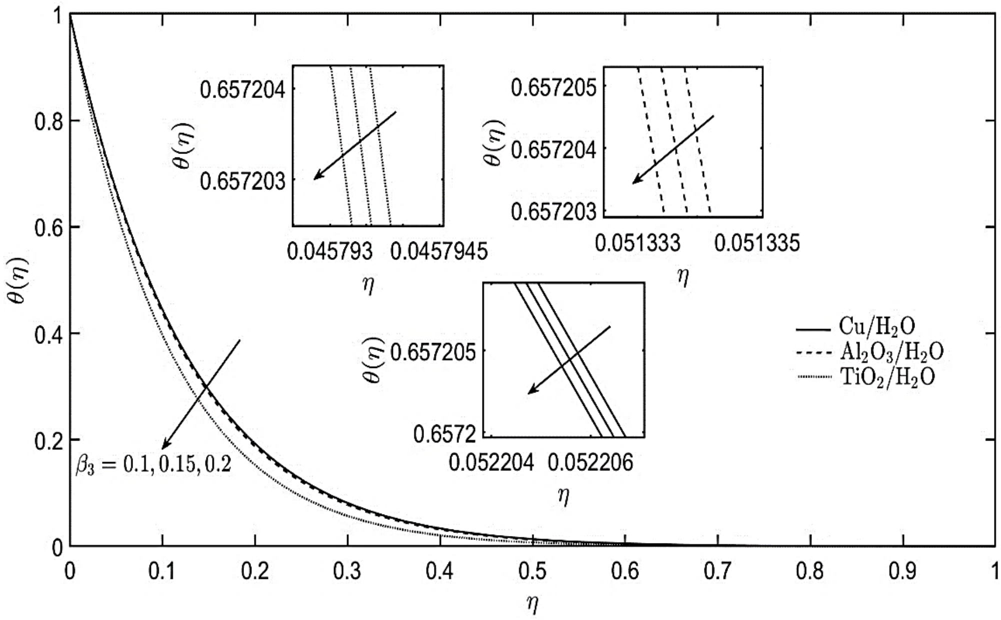

(**a**)

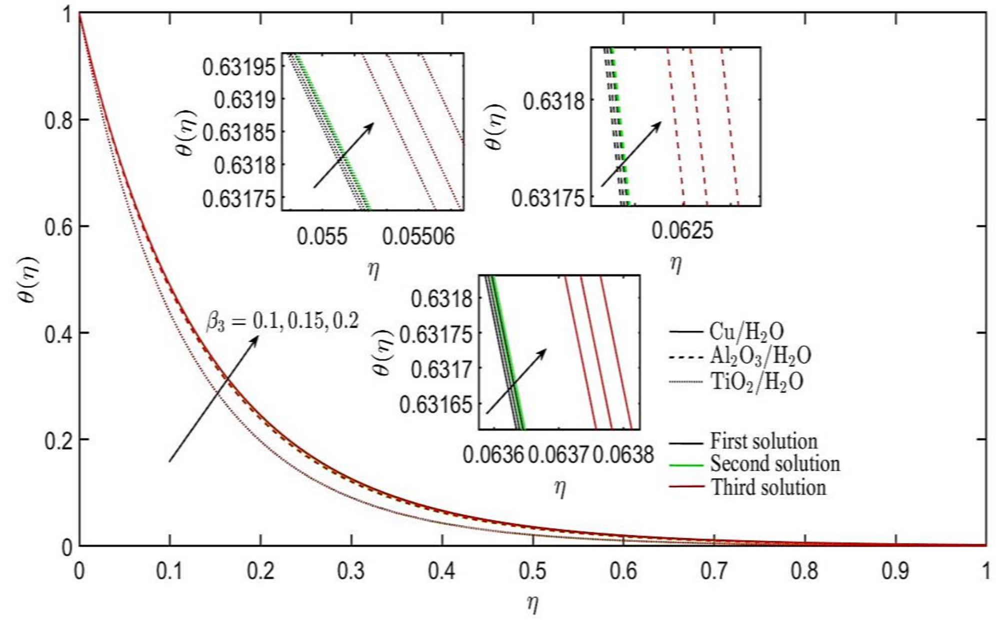

(**b**)

Figure 12. Effect of fluid retardation time parameter on temperature profiles for: (**a**) Stretching case; (**b**) Shrinking case.

5. Conclusions

The flow of various Burgers' nanofluids over a stretching/shrinking sheet in the presence of a heat source/sink is studied. The effects of nanoparticle volume fraction on the nanofluid flow are investigated by incorporating the Tiwari and Das nanofluid model in the problem formulation. Then, a built-in bvp4c package in MATLAB is utilized for numerical computation of the flow problem. The following are the significant findings of this study:

1. A unique solution is found for the stretching sheet case, while triple solutions are generated for the shrinking sheet case.
2. Stability analysis of solutions determined that only the first solution is stable and realizable in practice.

3. Three different nanofluids are considered, and Cu/H_2O nanofluid has the highest heat transfer rate compared to Al_2O_3/H_2O and TiO_2/H_2O nanofluids.
4. The application of Al_2O_3/H_2O and Cu/H_2O nanofluids in the flow over stretching and shrinking surfaces yield the highest skin friction coefficient, respectively.
5. The inclusion of more nanoparticles into the base fluid boosts the velocity and temperature profiles of the nanofluids.
6. The temperature profile is also augmented by the increment of the heat source parameter but diminished with the heat sink parameter.
7. The non-Newtonian parameters related to Burgers' fluid have different effects on the velocity and temperature profiles of the nanofluids for both cases of stretching and shrinking sheets.

This study can be extended to different flow geometries, such as Burgers' nanofluids flow over a stretching cylinder or between a cone and disk, and other physical conditions, such as entropy generation, variable concentration, and chemical reaction. Furthermore, this study can be expanded to suit the current application of heat transfer fluid, for example, in double pipe heat exchangers. Since this is a theoretical study, the experimental investigation of this flow problem is also encouraged.

Author Contributions: Conceptualization, I.P.; formal analysis, R.I.Y.; funding acquisition, N.M.A.; methodology, R.I.Y. and I.P.; supervision, N.M.A., F.M.A. and S.S.P.M.I.; validation, N.M.A. and I.P.; writing—original draft, R.I.Y. and I.P.; writing—review and editing, R.I.Y., N.M.A. and I.P. All authors have read and agreed to the published version of the manuscript.

Funding: This research was funded by Ministry of Higher Education Malaysia, grant number [KPT FRGS/1/2019/STG06/UPM/02/3, Vot 5540309].

Conflicts of Interest: The authors declare no conflict of interest. The funders had no role in the design of the study; in the collection, analyses, or interpretation of data; in the writing of the manuscript, or in the decision to publish the results.

Nomenclature

a	constant
C_f	skin friction coefficient
C_p	heat capacity (J/kgK)
f	dimensionless velocity
k	thermal conductivity (W/m·K)
K	heat source/sink parameter
$\boldsymbol{Nu_x}$	local Nusselt number
Pr	Prandtl number
Q_0	heat generation/absorption
Re_x	local Reynolds number
S	mass flux parameter
t	time (s)
T	fluid temperature (K)
x, y	Cartesian coordinates along the sheet and normal to it, respectively (m)
u, v	velocity components along the $\boldsymbol{x}$-and $\boldsymbol{y}$-directions, respectively (m/s)
U_w	velocity of the stretching/shrinking sheet (m/s)
v_w	mass transfer velocity (m/s)
Greek symbols	
$\beta_1, \beta_2, \beta_3$	non-Newtonian parameters
λ	stretching/shrinking parameter
λ_1	relaxation time
λ_2	material parameter
λ_3	retardation time
γ	unknown eigenvalue
η	similarity variable
ρ	fluid density (kg/m^3)

μ	dynamic viscosity (kg/m^{2}s)
τ	dimensionless time variable
ν	kinematic viscosity (m^2/s)
ψ	stream function
θ	dimensionless temperature
ϕ	nanoparticle volume fraction
Superscript	
$'$	differentiation with respect to η
Subscripts	
f	base fluid
n	nanofluid
s	nanoparticle
w	sheet surface
∞	free stream

References

1. Khan, M.; Iqbal, Z.; Ahmed, A. Energy transport analysis in the flow of burgers nanofluid inspired by variable thermal conductivity. *Pramana* **2021**, *95*, 74. https://doi.org/10.1007/s12043-021-02097-x.
2. Hayat, T.; Fetecau, C.; Asghar, S. Some simple flows of a burgers' fluid. *Int. J. Eng. Sci.* **2006**, *44*, 1423–1431. https://doi.org/10.1016/j.ijengsci.2006.08.008.
3. Rashidi, M.M.; Yang, Z.; Awais, M.; Nawaz, M.; Hayat, T. Generalized magnetic field effects in burgers' nanofluid model. *PLoS ONE* **2017**, *12*, e0168923. https://doi.org/10.1371/journal.pone.0168923.
4. Alsaedi, A.; Alsaadi, F.E.; Ali, S.; Hayat, T. Stagnation point flow of burgers' fluid and mass transfer with chemical reaction and porosity. *J. Mech.* **2012**, *29*, 453–460. https://doi.org/10.1017/jmech.2013.20.
5. Hayat, T.; Ali, S.; Awais, M.; Obaidat, S. Stagnation point flow of burgers' fluid over a stretching surface. *Prog. Comput. Fluid Dyn. Int. J.* **2013**, *13*, 48–53. https://doi.org/10.1504/PCFD.2013.050650.
6. Hayat, T.; Ali, S.; Awais, M.; Alsaedi, A. Joule heating effects in mhd flow of burgers' fluid. *Heat Transf. Res.* **2016**, *47*, 1083–1092. https://doi.org/10.1615/HeatTransRes.2016008093.
7. Hayat, T.; Asad, S.; Alaseadi, A. Mhd mixed convection flow of burgers' fluid in a thermally stratified medium. *J. Aerosp. Eng.* **2016**, 29, 04016060. https://doi.org/10.1061/(ASCE)AS.
8. Hayat, T.; Waqas, M.; Khan, M.I.; Alsaedi, A.; Shehzad, S.A. Magnetohydrodynamic flow of burgers fluid with heat source and power law heat flux. *Chin. J. Phys.* **2017**, *55*, 318–330. https://doi.org/10.1016/j.cjph.2017.02.004.
9. Ahmad, I.; Ali, N.; Abbasi, A.; Aziz, W.; Hussain, M.; Ahmad, M.; Taj, M.; Zaman, Q. Flow of a burger's fluid in a channel induced by peristaltic compliant walls. *J. Appl. Math.* **2014**, *2014*, 236483. https://doi.org/10.1155/2014/236483.
10. Khan, N.A.; Khan, S.; Ullah, S. Mhd flow of burger's fluid over an off-centered rotating disk in a porous medium. *AIP Adv.* **2015**, *5*, 087179. https://doi.org/10.1063/1.4929972.
11. Imran, M.; Ching, D.L.C.; Safdar, R.; Khan, I.; Imran, M.A.; Nisar, K.S. The solutions of non-integer order burgers' fluid flowing through a round channel with semi analytical technique. *Symmetry* **2019**, *11*, 962. https://doi.org/10.3390/sym11080962.
12. Safdar, R.; Imran, M.; Tahir, M.; Sadiq, N.; Imran, M.A. MHD Flow of Burgers' Fluid under the Effect of Pressure Gradient Through a Porous Material Pipe. *Punjab Univ. J. Math.* **2018**, *50*, 73–90.
13. Akram, S.; Anjum, A.; Khan, M.; Hussain, A. On stokes' second problem for burgers' fluid over a plane wall. *J. Appl. Comput. Mech.* **2021**, *7*, 1514–1526. https://doi.org/10.22055/jacm.2020.35227.2603.
14. Jiang, Y.; Sun, H.; Bai, Y.; Zhang, Y. MHD flow, radiation heat and mass transfer of fractional Burgers' fluid in porous medium with chemical reaction. *Comput. Math. Appl*. **2022**, *115*, 68–79. https://doi.org/10.1016/j.camwa.2022.01.014.
15. Gangadhar, K.; Kumari, M.A.; Rao, M.V.S.; Alnefaie, K.; Khan, I.; Andualem, M. Magnetization for burgers' fluid subject to convective heating and heterogeneous-homogeneous reactions. *Math. Probl. Eng.* **2022**, *2022*, 2747676. https://doi.org/10.1155/2022/2747676.
16. Choi, S.U.S.; Eastman, J.A. *Enhancing Thermal Conductivity of Fluids with Nanoparticles*; Argonne National Lab. (ANL): Argonne, IL, USA, 1995.
17. Alghamdi, M. Significance of arrhenius activation energy and binary chemical reaction in mixed convection flow of nanofluid due to a rotating disk. *Coatings* **2020**, *10*, 86. https://doi.org/10.3390/coatings10010086.
18. Khan, M.I.; Alzahrani, F. Activation energy and binary chemical reaction effect in nonlinear thermal radiative stagnation point flow of walter-b nanofluid: Numerical computations. *Int. J. Mod. Phys. B* **2020**, *34*, 2050132. https://doi.org/10.1142/S0217979220501325.
19. Hayat, T.; Waqas, M.; Shehzad, S.A.; Alsaedi, A. On model of burgers fluid subject to magneto nanoparticles and convective conditions. *J. Mol. Liq.* **2016**, *222*, 181–187. https://doi.org/10.1016/j.molliq.2016.06.087.
20. Hayat, T.; Waqas, M.; Shehzad, S.A.; Alsaedi, A. Mixed convection flow of a burgers nanofluid in the presence of stratifications and heat generation/absorption. *Eur. Phys. J. Plus* **2016**, *131*, 253. https://doi.org/10.1140/epjp/i2016-16253-9.

21. Iqbal, Z.; Khan, M.; Ahmed, A.; Ahmed, J.; Hafeez, A. Thermal energy transport in burgers nanofluid flow featuring the cattaneo–christov double diffusion theory. *Appl. Nanosci.* **2020**, *10*, 5331–5342. https://doi.org/10.1007/s13204-020-01386-y.
22. Xuan, Y.; Li, Q. Heat transfer enhancement of nanofluids. *Int. J. Heat Fluid Flow* **2000**, *21*, 58–64. https://doi.org/10.1016/S0142-727X(99)00067-3.
23. Das, S.K.; Choi, S.U.S.; Patel, H.E. Heat transfer in nanofluids—A review. *Heat Transf. Eng.* **2006**, *27*, 3–19. https://doi.org/10.1080/01457630600904593.
24. Khattak, M.A.; Mukhtar, A.; Afaq, S.K. Application of nano-fluids as coolant in heat exchangers: A review. *J. Adv. Res. Mater. Sci.* **2020**, *66*, 8–18. https://doi.org/10.37934/arms.66.1.818.
25. Das, S.K.; Choi, S.U.; Yu, W.; Pradeep, T. *Nanofluids: Science and Technology*; John Wiley & Sons: Hoboken, NJ, USA, 2007.
26. Nield, D.A.; Bejan, A. *Convection in Porous Media*; Springer: Berlin/Heidelberg, Germany, 2006; Volume 3.
27. Minkowycz, W.J.; Sparrow, E.M.; Abraham, J.P. *Nanoparticle Heat Transfer and Fluid Flow*; CRC Press: Boca Raton, FL, USA, 2012; Volume 4.
28. Shenoy, A.; Sheremet, M.; Pop, I. *Convective Flow and Heat Transfer from Wavy Surfaces: Viscous Fluids, Porous Media, and Nanofluids*; CRC Press: Boca Raton, FL, USA, 2016.
29. Manca, O.; Jaluria, Y.; Poulikakos, D. Heat Transfer in Nanofluids. *Advances in Mechanical Engineering*; Sage Publications: London, UK, 2010; p. 380826.
30. Myers, T.G.; Ribera, H.; Cregan, V. Does Mathematics Contribute to the Nanofluid Debate? *Int. J. Heat Mass Transf.* **2017**, *111*, 279–288. https://doi.org/10.1016/j.ijheatmasstransfer.2017.03.118.
31. Mahian, O.; Kolsi, L.; Amani, M.; Estellé, P.; Ahmadi, G.; Kleinstreuer, C.; Marshall, J.S.; Siavashi, M.; Taylor, R.A.; Niazmand, H.; et al. Recent advances in modeling and simulation of nanofluid flows-part i: Fundamentals and theory. *Phys. Rep.* **2019**, *790*, 1–48. https://doi.org/10.1016/j.physrep.2018.11.004.
32. Mahian, O.; Kolsi, L.; Amani, M.; Estellé, P.; Ahmadi, G.; Kleinstreuer, C.; Marshall, J.S.; Taylor, R.A.; Abu-Nada, E.; Rashidi, S. Recent advances in modeling and simulation of nanofluid flows—Part II: Applications. *Phys. Rep.* **2019**, *791*, 1–59.
33. Mahian, O.; Kianifar, A.; Kalogirou, S.A.; Pop, I.; Wongwises, S. A review of the applications of nanofluids in solar energy. *Int. J. Heat Mass Transf.* **2013**, *57*, 582–594. https://doi.org/10.1016/j.ijheatmasstransfer.2012.10.037.
34. Khan, M.; Khan, W.A. Forced convection analysis for generalized Burgers nanofluid flow over a stretching sheet. *AIP Adv.* **2015**, *5*, 107138. https://doi.org/10.1063/1.4935043.
35. Khan, M.; Khan, W.A. Steady flow of Burgers' nanofluid over a stretching surface with heat generation/absorption. *J Braz. Soc. Mech. Sci. Eng.* **2016**, *38*, 2359–2367. https://doi.org/10.1007/s40430-014-0290-4.
36. Buongiorno, J. Convective transport in nanofluids. *J. Heat Transf.* **2006**, *128*, 240–250. https://doi.org/10.1115/1.2150834.
37. Muhammad, S.; Ishaq, M.; Hussain, S.A.; Tahir, M.; Naeem, M.; Khan, H.; Jan, S.; Khan, K. Semi analytical solution of steady Burgers' nanofluid flow between parallel channels with heat generation/absorption under the influence of thermal radiation. *J. Nanofluids* **2019**, *8*, 1468–1478. https://doi.org/10.1166/jon.2019.1706.
38. Khan, M.; Iqbal, Z.; Ahmed, A. Stagnation point flow of magnetized burgers' nanofluid subject to thermal radiation. *Appl. Nanosci.* **2020**, *10*, 5233–5246. https://doi.org/10.1007/s13204-020-01360-8.
39. Khan, S.U.; Alabdan, R.; Al-Qawasmi, A.-R.; Vakkar, A.; ben Handa, M.; Tlili, I. Bioconvection applications for double stratification 3-d flow of burgers nanofluid over a bidirectional stretched surface: Enhancing energy system performance. *Case Stud. Therm. Eng.* **2021**, *26*, 101073. https://doi.org/10.1016/j.csite.2021.101073.
40. Waqas, H.; Manzoor, U.; Shah, Z.; Arif, M.; Shutaywi, M. Magneto-burgers nanofluid stratified flow with swimming motile microorganisms and dual variables conductivity configured by a stretching cylinder/plate. *Math. Probl. Eng.* **2021**, *2021*, 8817435. https://doi.org/10.1155/2021/8817435.
41. Ramzan, M.; Algehyne, E.A.; Saeed, A.; Dawar, A.; Kumam, P.; Watthayu, W. Homotopic simulation for heat transport phenomenon of the Burgers nanofluids flow over a stretching cylinder with thermal convective and zero mass flux conditions. *Nanotechnol. Rev.* **2022**, *11*, 1437–1449. https://doi.org/10.1515/ntrev-2022-0089.
42. Wang, F.; Iqbal, Z.; Zhang, J.; Abdelmohimen, M.A.H.; Almaliki, A.H.; Galal, A.M. Bidirectional stretching features on the flow and heat transport of Burgers nanofluid subject to modified heat and mass fluxes. *Waves Random Complex Media* **2022**, 1–18. https://doi.org/10.1080/17455030.2022.2055203.
43. Tiwari, R.K.; Das, M.K. Heat transfer augmentation in a two-sided lid-driven differentially heated square cavity utilizing nanofluids. *Int. J. Heat Mass Transf.* **2007**, *50*, 2002–2018. https://doi.org/10.1016/j.ijheatmasstransfer.2006.09.034.
44. Pop, I.; Seddighi, S.; Bachok, N.; Ismail, F. Boundary layer flow beneath a uniform free stream permeable continuous moving surface in a nanofluid. *J. Heat Mass Transf. Res.* **2014**, *1*, 55–65. https://doi.org/10.22075/jhmtr.2014.154.
45. Ejaz, A.; Abbas, I.; Nawaz, Y.; Arif, M.S.; Shatanawi, W.; Abbasi, J.N. Thermal analysis of mhd non-newtonian nanofluids over a porous media. *CMES—Comput. Model. Eng. Sci.* **2020**, *125*, 1119–1134. https://doi.org/10.32604/cmes.2020.012091.
46. Ho, C.J.; Liu, W.K.; Chang, Y.S.; Lin, C.C. Natural convection heat transfer of alumina-water nanofluid in vertical square enclosures: An experimental study. *Int. J. Therm. Sci.* **2010**, *49*, 1345–1353. https://doi.org/10.1016/j.ijthermalsci.2010.02.013.
47. Sheremet, M.A.; Pop, I.; Rosca, A.V. The influence of thermal radiation on unsteady free convection in inclined enclosures filled by a nanofluid with sinusoidal boundary conditions. *Int. J. Numer. Methods Heat Fluid Flow* **2018**, *28*, 1738–1753. https://doi.org/10.1108/HFF-09-2017-0375.
48. Oztop, H.F.; Abu-Nada, E. Numerical study of natural convection in partially heated rectangular enclosures filled with nanofluids. *Int. J. Heat Fluid Flow* **2008**, *29*, 1326–1336. https://doi.org/10.1016/j.ijheatfluidflow.2008.04.009.

49. Fang, T.; Yao, S.; Zhang, J.; Aziz, A. Viscous flow over a shrinking sheet with a second order slip flow model. *Commun. Nonlinear Sci. Numer. Simul.* **2010**, *15*, 1831–1842. https://doi.org/10.1016/j.cnsns.2009.07.017.
50. Vajravelu, K.; Rollins, D. Hydromagnetic flow of a second grade fluid over a stretching sheet. *Appl. Math. Comput.* **2004**, *148*, 783–791. https://doi.org/10.1016/S0096-3003(02)00942-6.
51. Cortell, R. Viscous flow and heat transfer over a nonlinearly stretching sheet. *Appl. Math. Comput.* **2007**, *184*, 864–873. https://doi.org/10.1016/j.amc.2006.06.077.
52. Crane, L.J. Flow past a stretching plate. *Z. Angew. Math. Phys. ZAMP* **1970**, *21*, 645–647. https://doi.org/10.1007/BF01587695.
53. Weidman, P.D.; Kubitschek, D.G.; Davis, A.M.J. The effect of transpiration on self-similar boundary layer flow over moving surfaces. *Int. J. Eng. Sci.* **2006**, *44*, 730–737. https://doi.org/10.1016/j.ijengsci.2006.04.005.
54. Roşca, A.V.; Pop, I. Flow and heat transfer over a vertical permeable stretching/shrinking sheet with a second order slip. *Int. J. Heat Mass Transf.* **2013**, *60*, 355–364. https://doi.org/10.1016/j.ijheatmasstransfer.2012.12.028.
55. Wahid, N.S.; Arifin, N.M.; Khashi'ie, N.S.; Pop, I. Hybrid nanofluid slip flow over an exponentially stretching/shrinking permeable sheet with heat generation. *Mathematics* **2020**, *9*, 30. https://doi.org/10.3390/math9010030.
56. Lund, L.A.; Omar, Z.; Khan, U.; Khan, I.; Baleanu, D.; Nisar, K.S. Stability analysis and dual solutions of micropolar nanofluid over the inclined stretching/shrinking surface with convective boundary condition. *Symmetry* **2020**, *12*, 74. https://doi.org/10.3390/sym12010074.
57. Yahaya, R.I.; Md Arifin, N.; Mohamed Isa, S.S.P.; Rashidi, M.M. Magnetohydrodynamics boundary layer flow of micropolar fluid over an exponentially shrinking sheet with thermal radiation: Triple solutions and stability analysis. *Math. Methods Appl. Sci.* **2021**, *44*, 10578–10608. https://doi.org/10.1002/mma.7432.
58. Harris, S.D.; Ingham, D.B.; Pop, I. Mixed convection boundary-layer flow near the stagnation point on a vertical surface in a porous medium: Brinkman model with slip. *Transp. Porous Media* **2009**, *77*, 267–285. https://doi.org/10.1007/s11242-008-9309-6.
59. Zainal, N.A.; Nazar, R.; Naganthran, K.; Pop, I. Stability analysis of unsteady mhd rear stagnation point flow of hybrid nanofluid. *Mathematics* **2021**, *9*, 2428. https://doi.org/10.3390/math9192428.
60. Khashi'ie, N.S.; Arifin, N.M.; Merkin, J.H.; Yahaya, R.I.; Pop, I. Mixed convective stagnation point flow of a hybrid nanofluid toward a vertical cylinder. *Int. J. Numer. Methods Heat Fluid Flow* **2021**, *31*, 3689–3710. https://doi.org/10.1108/HFF-11-2020-0725.
61. Yahaya, R.I.; Md Arifin, N.; Nazar, R.M.; Pop, I. Oblique stagnation-point flow past a shrinking surface in a Cu-Al_2O_3/H_2O hybrid nanofluid. *Sains Malays.* **2021**, *50*, 3139–3152. https://doi.org/10.17576/jsm-2021-5010-25.
62. Pantokratoras, A. A common error made in investigation of boundary layer flows. *Appl. Math. Model.* **2009**, *33*, 413–422. https://doi.org/10.1016/j.apm.2007.11.009.
63. Rahman, M.M.; Ariz, A. Heat transfer in water based nanofluids (TiO_2-H_2O, Al_2O_3-H_2O and Cu-H_2O) over a stretching cylinder. *Int. J. Heat Technol*. **2012**, *30*, 31–42. https://doi.org/10.18280/ijht.300205.
64. Dawar, A.; Bonyah, E.; Islam, S.; Alshehri, A.; Shah, Z. Theoretical analysis of Cu-H_2O, Al_2O_3-H_2O, and TiO_2-H_2O nanofluid flow past a rotating disk with velocity slip and convective conditions. *J. Nanomater.* **2021**, *2021*, 5471813. https://doi.org/10.1155/2021/5471813.